

Identification of interstellar amino acetonitrile in the hot molecular core G10.47+0.03: Possible glycine survey candidate for the future

Arijit Manna^a, Sabyasachi Pal^{a,*}

^aMidnapore City College, Kuturia, Bhadutala, Paschim Medinipur, West Bengal, India 721129

ARTICLE INFO

Keywords:

ISM: individual objects (G10.47+0.03)

ISM: abundances

ISM: kinematics and dynamics

stars: formation

Astrochemistry

ABSTRACT

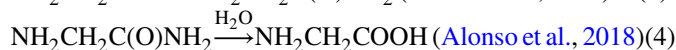
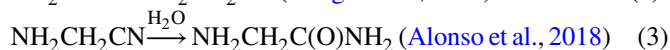
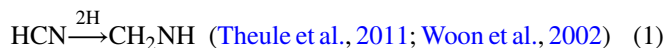
Amino acids are the essential keys that contribute to the study of the formation of life. The simplest amino acid, glycine ($\text{NH}_2\text{CH}_2\text{COOH}$), has been searched for a long time in the interstellar medium, but all surveys of glycine have failed. Since the detection of glycine in the interstellar medium was extremely difficult, we aimed to search for the precursor of glycine. After detailed searches of the individual prebiotic molecular species, we successfully identified the emission lines of possible glycine precursor molecule amino acetonitrile ($\text{NH}_2\text{CH}_2\text{CN}$) towards the hot molecular core G10.47+0.03 using the Atacama Large Millimeter/Submillimeter Array. We estimated the statistical column density of amino acetonitrile was $(9.10 \pm 0.7) \times 10^{15} \text{ cm}^{-2}$ with rotational temperature (T_{rot}) $122 \pm 8.8 \text{ K}$. The estimated fractional abundance of amino acetonitrile was 7.01×10^{-8} . We found that the estimated fractional abundance of $\text{NH}_2\text{CH}_2\text{CN}$ fairly agrees with the theoretical value predicted by the three-phase warm-up model from Garrod (2013).

1. Introduction

In the interstellar medium, more than 260 molecules have been detected using the millimeter/submillimeter radio telescopes¹. The hot molecular cores are chemically rich complex systems in the interstellar medium, and several complex organic molecules have been detected in the hot molecular core regions (Garrod et al., 2017; Belloche et al., 2016; Gorai et al., 2020; Manna & Pal, 2021). In this article, we give priority to the study of prebiotic organic molecular spectral lines towards the hot molecular core region G10.47+0.03 (hereafter, G10), which was observed at a distance of 8.6 kpc (Sanna et al., 2014). The luminosity of the hot molecular core G10 was $10^6 L_{\odot}$, which indicates that G10 is one of the highest luminosity star-forming region in the galaxy and particularly interesting to the investigation of the molecular lines (Roloffs et al., 2009). The emission lines of NH_2CHO , CH_3NCO , and HNCO were detected towards G10 using the Atacama Large Millimeter/Submillimeter Array (Gorai et al., 2020). Recently, the complex molecular emission lines of CH_3OH , $(\text{CH}_2\text{OH})_2$, CH_3CHO , $\text{CH}_3\text{CH}_2\text{CHO}$, HOCH_2CHO , CH_3COCH_3 , CH_3OCHO , and CH_3OCH_3 were also detected towards G10 using the ALMA (Mondal et al., 2021). Earlier, the emission lines of prebiotic complex molecules methanimine (CH_2NH) and methylamine (CH_3NH_2) were detected towards G10, which are the simplest imine and amine, respectively (Suzuki et al., 2016; Ohishi et al., 2019). The prebiotic molecule CH_3NH_2 plays an important role in the formation of the glycine isomer CH_3NHCOOH towards the hot molecular cores (Holtom et al., 2005). The bio-molecule CH_3NH_2 will be produced during the warm-up phases between the reactions of NH_2 and CH_3 under cosmic ray irradiation on the grain surface ($\text{NH}_2 + \text{CH}_3 \rightarrow \text{CH}_3\text{NH}_2$) (Kim & Kaiser, 2011). When CH_3NH_2 molecule reacts with CO_2 under UV irradiation, it forms the glycine isomer molecule

CH_3NHCOOH in the solid phase ($\text{CH}_3\text{NH}_2 \xrightarrow{\text{CO}_2} \text{CH}_3\text{NHCOOH}$) (Holtom et al., 2005). In another way, CH_3NH_2 molecule can be produced in the interstellar medium due to hydrogenation of HCN on the dust surface of hot molecular cores ($\text{HCN} \xrightarrow{2\text{H}} \text{CH}_2\text{NH} \xrightarrow{2\text{H}} \text{CH}_3\text{NH}_2$) (Theule et al., 2011). As two possible precursors of glycine CH_3NH_2 and CH_2NH were already detected towards G10 (Ohishi et al., 2019; Suzuki et al., 2016), we tried to search for another prebiotic molecule, amino acetonitrile ($\text{NH}_2\text{CH}_2\text{CN}$) towards G10, which was known as another possible precursor of glycine (Brown et al., 1977; Elsila et al., 2007; Ohishi et al., 2019).

The complex nitrile molecule amino acetonitrile (hereafter, AAN) is known as one of the important rare compounds in the interstellar medium, which is also known as glycine nitrile (Wirström et al., 2007). The AAN molecule is one of the important species for astrochemists and astrobiologists because AAN can be converted into glycine after hydrolysis via glycinamide ($\text{NH}_2\text{CH}_2(\text{O})\text{NH}_2$) (Alonso et al., 2018; Peltzer et al., 1984; Wirström et al., 2007). Earlier, astrochemists suggested the possible chemical pathways for the formation of glycine from AAN via glycinamide on the dust surface of the hot molecular cores:



Reaction 1 indicated that the CH_2NH molecule was produced on the dust surface via the hydrogenation of HCN (Theule et al., 2011; Woon et al., 2002). Reaction 2 presented the formation pathways of AAN between the reactions of CH_2NH and HCN via the Strecker synthesis reaction (Danger et al., 2011). Now, in the interstellar medium, the hydrolysis of AAN in the gas phase or the icy mantle on the grain sur-

ORCID(s):

¹<https://cdms.astro.uni-koeln.de/classic/molecules>

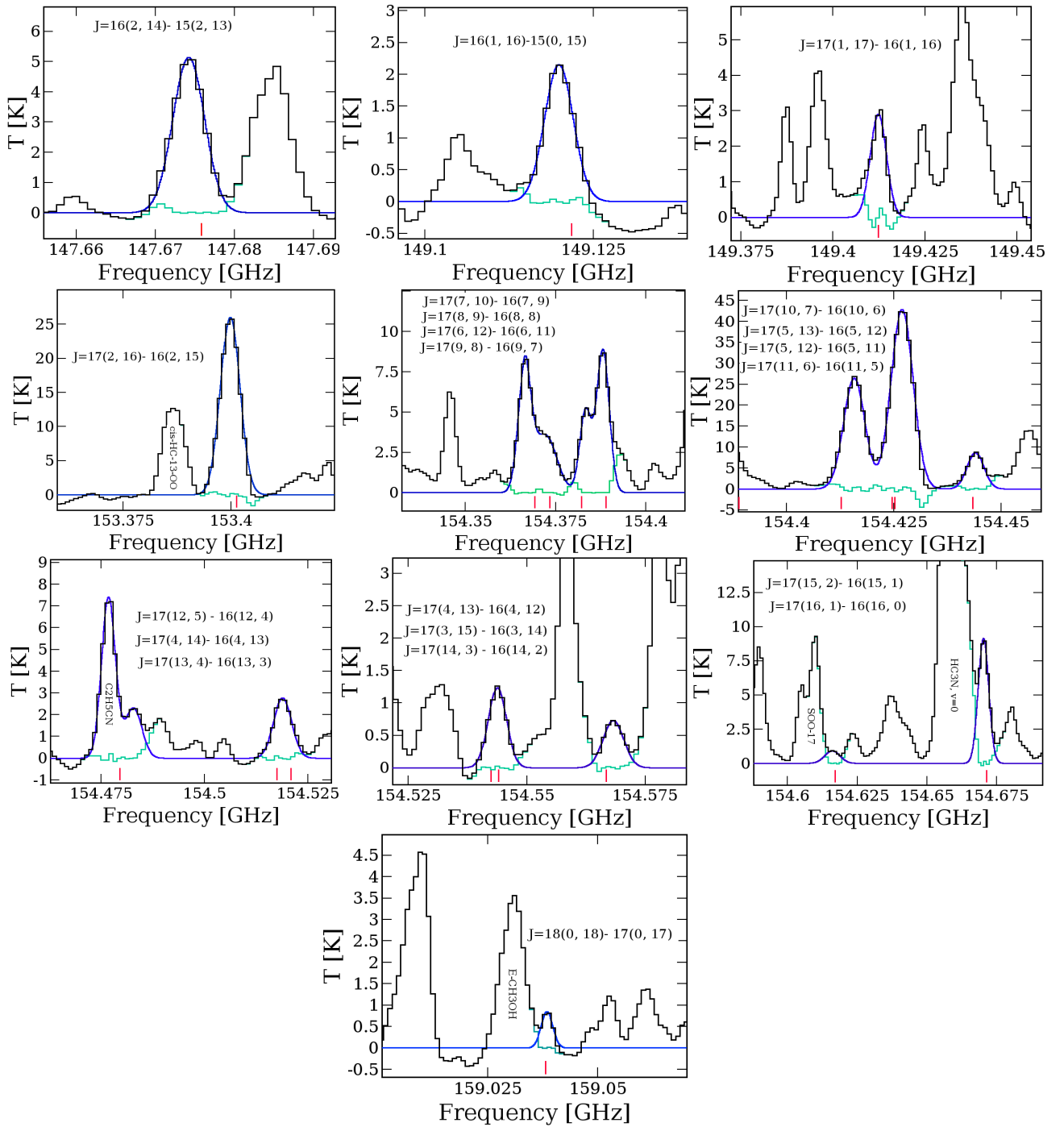


Figure 1: Rotational emission spectra of AAN with different molecular transitions towards G10. From the emission spectra, the continuum emission was completely subtracted. The black line showed the observed spectra, while the blue line showed the Gaussian model, which was overlaid on the observed spectra of AAN. The green spectra indicated the residual. The red lines indicate the peak position of the detected transitions of AAN.

face produces glycnamide ($\text{NH}_2\text{CH}_2\text{C}(\text{O})\text{NH}_2$), as shown in reaction 3 (Alonso et al., 2018). The hydrolysis of glycnamide forms glycine on the grain surface, which was presented in reactions 4 (Alonso et al., 2018). Recently, Kisiel et al. (2022) searched for the emission lines of glycnamide from Sgr B2(N) but they cannot find any evidence of glycnamide within the limit of the Local Thermodynamic Equi-

librium (LTE) model. They estimated the upper limit column density of glycnamide towards Sgr B2(N) was $\leq 1.5 \times 10^{16} \text{ cm}^{-2}$. Earlier, Koch et al. (2008) found that H_2O can efficiently catalyze a reaction between CH_2NH and HNC to form AAN in the grain mantles at a temperature of 50 K. The AAN molecule contains both amino and nitrile groups (Sharma, 2019). The survival of AAN against UV photoly-

Table 1
Summary of the line parameters of the AAN towards G10.

Frequency range (GHz)	Observed frequency (GHz)	Transition ($J'_{K'_a K'_c} - J''_{K''_a K''_c}$) [†]	E_u (K)	A_{ij} (s^{-1})	Peak intensity (K)	S_{μ}^2 (Debye ²)	FWHM (km s ⁻¹)	$\int T_{mb} dv$ (K km s ⁻¹)	V_{LSR} (km s ⁻¹)	Remark
147.55–148.01 [⊙]	147.6758	16(2,14)–15(2,13) [†]	64.76	1.19×10 ⁻⁴	5.081	104.623	5.262±0.62	40.629±4.56	68.607	blended with c-HCC ¹³ CH
148.50–149.43 [⊙]	149.1218	16(1,16)–15(0,15)	58.79	4.50×10 ⁻⁶	2.123	3.8437	6.653±0.98	20.824±3.16	68.820	blended with c-C ₃ H ₂
	149.4123	17(1,17)–16(1,16)	65.96	1.25×10 ⁻⁴	3.014	112.419	4.582±0.32	31.425±2.56	68.506	Detected
153.00–153.93 [⊙]	153.4012	17(2,16)–16(2,15)	71.37	1.34×10 ⁻⁴	25.778	111.262	6.286±0.97	232.587±12.69	68.589	blended with CH ₃ CHO
154.0–154.93 [⊙]	154.3692	17(7,10)–16(7,9) ^{**}	127.05	1.15×10 ⁻⁴	4.753	93.746	6.975±0.63	72.498±10.32	68.692	blended with c-HCC ¹³ CN
	154.3734	17(8,9)–16(8,8) ^{**}	145.50	1.08×10 ⁻⁴	3.234	87.892	5.628±0.78	96.558±19.39	68.596	blended with SO ₂
	154.3822	17(6,12)–16(6,11) ^{**}	111.04	1.021×10 ⁻⁴	4.645	98.835	5.698±0.43	34.261±3.97	68.521	blended with SO ¹⁸ O and NH ₂ D
	154.3889	17(9,8)–16(9,7) ^{**}	146.41	9.95×10 ⁻⁵	8.984	81.250	5.889±0.97	103.936±20.39	68.561	blended with E-CH ₃ OH
	154.4128	17(10,7)–16(10,6) ^{**}	189.75	9.04×10 ⁻⁵	26.713	73.837	6.823±1.26	258.351±42.93	68.643	blended with HNCO
	154.4246	17(5,13)–16(5,12) [†]	97.50	1.26×10 ⁻⁴	42.224	103.125	6.956±0.86	321.989±60.29	68.597	blended with E-CH ₃ OH
	154.4252	17(5,12)–16(5,11) [†]	97.50	1.26×10 ⁻⁴	42.224	103.124	6.958±0.87	321.998±60.35	68.597	blended with E-CH ₃ OH
	154.4433	17(11,6)–16(11,5) ^{**}	215.52	8.04×10 ⁻⁵	8.783	65.630	4.805±0.69	64.882±10.36	68.563	blended with HC ₃ N
	154.4796	17(12,5)–16(12,4) ^{**}	243.71	6.95×10 ⁻⁵	2.814	56.638	4.207±0.67	46.244±12.16	68.543	blended with C ₂ H ₅ CN
	154.5175	17(4,14)–16(4,13) [†]	86.42	1.31×10 ⁻⁴	2.695	106.637	4.221±0.34	33.667±2.96	68.537	Detected
	154.5209	17(13,4)–16(13,3) ^{**}	274.31	5.75×10 ⁻⁵	2.695	46.879	4.221±0.34	33.667±2.94	68.537	Detected
	154.5424	17(4,13)–16(4,12) [†]	86.43	1.31×10 ⁻⁴	1.269	106.653	4.821±0.98	66.107±5.16	68.594	blended with U line
	154.5440	17(3,15)–16(3,14) [†]	77.81	1.34×10 ⁻⁴	1.269	109.368	4.821±0.98	66.107±5.19	68.594	blended with U line
	154.5666	17(14,3)–16(14,2) [†]	307.31	4.46×10 ⁻⁵	0.758	36.333	4.536±0.78	97.258±9.83	68.439	Detected
	154.6170	17(15,2)–16(15,1) ^{**}	342.71	3.07×10 ⁻⁵	0.953	25.001	4.789±0.62	8.595±2.69	68.396	blended with c-C ₃ H
	154.6714	17(16,1)–16(16,0)	380.48	1.59×10 ⁻⁵	8.863	12.892	5.537±0.68	86.402±12.98	68.513	blended with HC ₃ N
158.49–159.43 [⊙]	159.0381	18(0,18)–17(0,17)	73.29	1.51×10 ⁻⁴	0.814	119.204	4.823±0.32	3.791±0.97	68.509	Detected

[†] – Those transitions of AAN were also detected in Sgr B2 (Belloche et al., 2008).

* – Transitions contain double with frequency difference less than 100 kHz. The quantum numbers of the second are not shown.

⊙ – Spectral resolution 488.28 kHz

⊗ – Spectral resolution 1128.91 kHz

sis in the interstellar ices was ~ 5 times longer than glycine (Bernstein et al., 2004). Earlier, Wirström et al. (2007) did not find the molecular lines of AAN from hot molecular cores Orion KL, W51 e1/e2, S140, and W3(OH) using the Onsala 20 m telescope. The emission lines of interstellar AAN were first time detected towards Sgr B2(N) with column density 2.8×10^{16} cm⁻² and excitation temperature 100 K using IRAM, and later the emission lines of AAN in Sgr B2(N) was verified by ATCA and VLA (Belloche et al., 2008). Recently, astrochemists tried to search for the emission lines of AAN and glycine towards the quiescent giant molecular cloud G+0.693–0.027 and hot corino IRAS 16293–2422 B but they did not detect them within the LTE approximation (Jiménez et al., 2020). After the non detection of AAN from G+0.693–0.027 and IRAS 16293–2422 B, Jiménez et al. (2020) estimated the upper limit column density of AAN in G+0.693–0.027 and IRAS 16293–2422 B was $\leq 0.6 \times 10^{13}$ cm⁻² and $\leq 1.2 \times 10^{14}$ cm⁻² respectively. The electric dipole moment of AAN is $\mu_a = 2.577$ D and $\mu_b = 0.5754$ D which indicates that the a-type transitions are 20 times higher than b-types transitions (Pickett, 1973; Sharma, 2019).

In this article, we presented the first interferometric detection of complex amino and nitrile mixed molecule AAN towards the hot molecular core G10 using ALMA. We used the rotational diagram method under the LTE conditions to calculate the column density (N) and rotational temperature (T_{rot}) of the emission lines of AAN. We also compared our estimated abundance of AAN with the three-phase warm-up model of Garrod (2013). The ALMA observation and data reduction were presented in Section 2. The result of the detection of emission lines of AAN was shown in Section 3. The discussion and conclusion of the detection of AAN were shown in Section 4 and 5.

2. Observations and data reductions

The hot molecular core G10 was observed to study the interstellar complex organic prebiotic molecules using the high-resolution Atacama Large Millimeter/submillimeter Array (ALMA)² with band 4 in cycle 4. The hot molecular core G10 was observed on 28th January 2017, 5th March 2017, 6th March 2017, and 7th March 2017 with phase center of $(\alpha, \delta)_{J2000} = (18:08:38.232, -19:51:50.400)$. The on-source integration time on these days was 2026.080 sec, 3810.240 sec, 6804.000 sec, and 1723.680 sec, respectively, and a total of thirty-nine, forty, forty-one, and thirty-nine antennas were used during these observations. The observation aimed to study five-strong emission lines of interstellar glycine towards G10. The observations of G10 were carried out in four spectral windows with frequency ranges 129.50–134.44 GHz, 147.50–149.43 GHz, 153.00–154.93 GHz, and 158.49–160.43 GHz with a spectral resolution of 1128.91 kHz and 488.28 kHz. The angular resolution of different frequency ranges was 1.67'' (14362 AU), 1.52'' (13072 AU), 1.66'' (14276 AU), and 1.76'' (15136 AU) respectively. During the observation, J1733–1304, J1832–2039, and J1924–2914 were used as flux calibrator, phase calibrator, and bandpass calibrator respectively. The systemic velocity (V_{LSR}) of G10 is ~ 68.50 km s⁻¹ (Rolffs et al., 2011).

For initial data reduction and spectral imaging, we used the Common Astronomy Software Application (CASA 5.4.1) with the standard ALMA data reduction pipeline (McMullin et al., 2007). During the analysis of the raw data of G10, the continuum flux density of the flux calibrator for each baseline was scaled and matched with the Perley-Butler 2017 flux calibrator model with 5% accuracy using task SETJY (Perley & Butler, 2017). We made flux and bandpass calibration after discarding the bad data using CASA pipeline with task

²<https://almascience.nao.ac.jp/asax/>

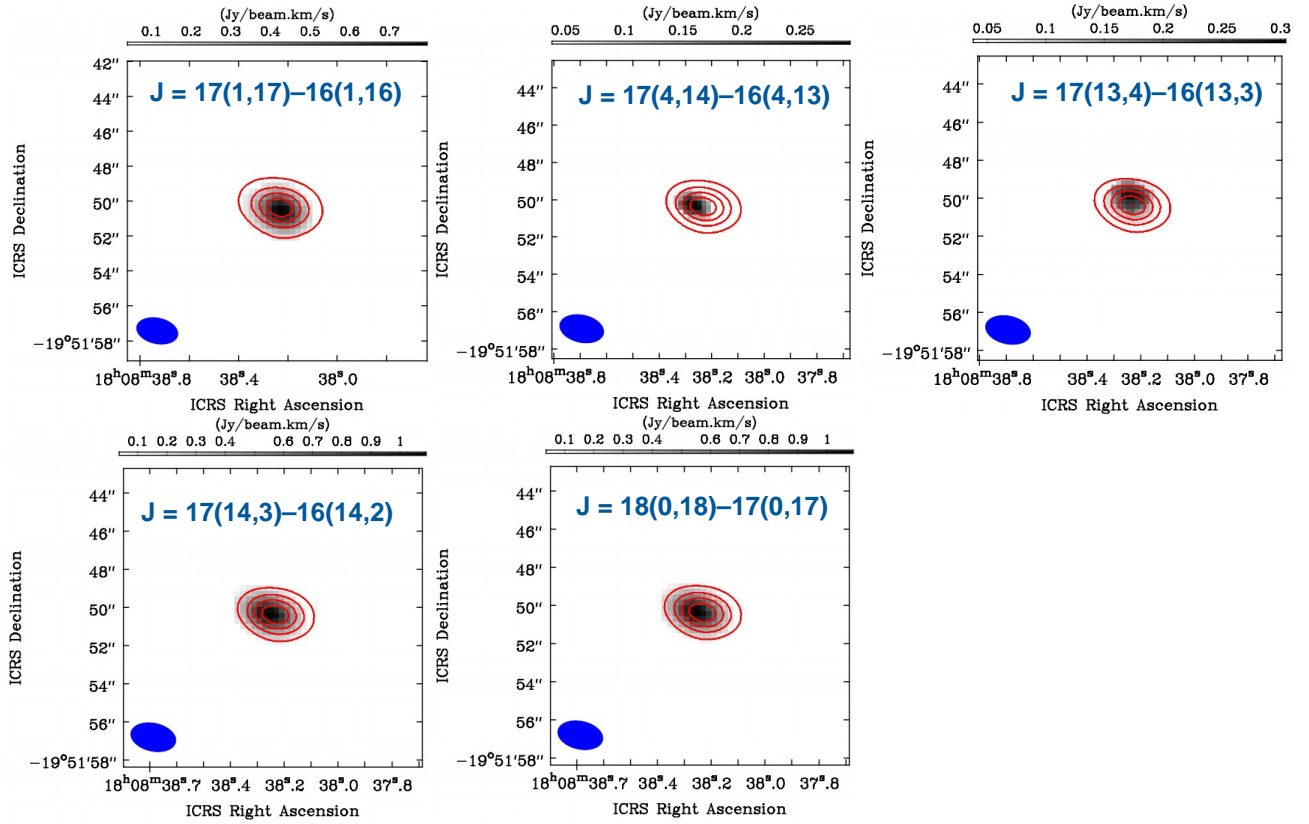


Figure 2: The integrated emission map of unblended transitions of AAN towards G10 which was overlaid with the 1.87 mm continuum emission (red contour). Contour levels are at 20%, 40%, 60%, and 80% of the peak flux. The blue circle indicated the synthesized beam of the integrated map.

hifa_bandpassflag and hifa_flagdata. After the initial calibration, we split the target data set into another data set using task MSTRANSFORM with all available rest frequencies. For the continuum subtraction procedure, we used the task UVCONTSUB in the UV plane of split calibrated data. We generated the spectral datacubes of G10 using task TCLEAN for each rest frequency with a Briggs weighting robust parameter of 0.5. For the correction of the primary beam pattern in the synthesized image, we applied the IMPBCOR task in CASA. Earlier, [Gorai et al. \(2020\)](#) presented a detailed description of the observations of the hot molecular core G10 using ALMA.

3. Result

3.1. Analysis of the emission lines of interstellar AAN towards G10

We extracted the sub-millimeter spectra of hot molecular core G10 from the continuum subtracted spectral data cubes to make a $2.5''$ diameter circular region at the center of RA (J2000) = ($18^h08^m38^s.232$), Dec (J2000) = ($-19^\circ51'50''.440$). The systematic velocity of the sub-millimeter spectra towards G10 was 68.50 km s^{-1} . After the extraction of the sub-millimeter spectrum, we used CASSIS ([Vas- tel et al., 2015](#)) for the identification of the emission lines of interstellar molecules towards G10. After careful spectral analysis, we identified the emission lines of the complex

organic molecule AAN (a-type), which was known as a possible precursor of glycine. We used the Cologne Database for Molecular Spectroscopy (CDMS)³ ([Müller et al., 2005](#)) to identify the emission lines of AAN. The hot molecular core G10 was chemically very rich and the detection of AAN was extremely difficult due to contamination of other nearby molecular lines. We detected a total of twenty-one rotational transition lines of AAN between the frequency ranges of 147.55–148.01 GHz, 148.50–149.43 GHz, 153.00–153.93 GHz, 154.0–154.93 GHz, and 158.49–159.43 GHz towards G10.

After the identification of emission lines of AAN from the submillimeter spectra of G10, we fitted the Gaussian model over the observed spectra of AAN using the line analysis module in CASSIS. After the fitting of Gaussian model over the observed spectra of AAN, we estimated the Full-Width Half Maximum (FWHM), quantum numbers ($J'_{K'_a K'_c} - J''_{K''_a K''_c}$), upper state energy (E_u), Einstein coefficients (A_{ij}), peak intensity and integrated intensity ($\int T_{\text{mb}} dV$). There was no missing a-type transition of AAN in this data. The summary of the observed transitions of AAN and Gaussian fitting of spectral parameters were presented in Table 1 and the observed spectra of AAN with the best fitting Gaussian model were shown in Figure 1. Earlier, the emission lines of AAN

³<https://cdms.astro.uni-koeln.de/cgi-bin/cdmssearch>

Table 2

Summary of 2D Gaussian fitting parameters over the integrated emission map of AAN

Transition [$J'_{K'_a K'_c} - J''_{K''_a K''_c}$]	Integrated flux [Jy.km s ⁻¹]	Peak flux [Jy beam ⁻¹ . km s ⁻¹]	Emitting region [$''$]	Position angle [$^\circ$]
17(1,17)–16(1,16)	1.179±0.29	0.826±0.02	1.12	77.960
17(4,14)–16(4,13)	0.830±0.06	0.733±0.04	1.13	77.971
17(13,4)–16(13,3)	0.741±0.09	0.607±0.03	1.11	77.960
17(14,3)–16(14,2)	1.805±0.59	1.248±0.65	1.12	77.968
18(0,18)–17(0,17)	1.386±0.76	1.174±0.98	1.12	77.968

were first detected from Sgr B2(N) using the IRAM 30 m single-dish radio telescope (Belloche et al., 2008). The spectral linewidth of observed emission lines of AAN towards Sgr B2(N) was ~ 7 km s⁻¹ (Belloche et al., 2008). So, there was a high probability of the contamination of other nearby molecular transitions with AAN towards Sgr B2(N) whereas our detected spectral width of AAN towards G10 was found between the range of 4–6 km s⁻¹. Our observed maximum transition lines of AAN towards G10 were blended with other nearby molecular lines because the observed transitions of AAN did not resolve due to the low spectral resolution. Our identified transitions of AAN between the frequency range of 147.55–148.01 GHz and 154.0–154.93 GHz towards G10 were also detected towards Sgr B2(N) by IRAM (Belloche et al., 2008).

3.2. Spatial distribution of AAN

After the identification of the emission lines of AAN towards G10, we extracted the integrated emission map of AAN using task `IMMOMENTS` in `CASA`, which was shown in Figure 2. The integrated emission map of AAN was overlaid with the 1.87 mm continuum emission map of G10⁴. We also observed that the emission map of AAN has a peak at the position of the continuum. The integrated emission maps were generated by integrating the spectral data cubes in the velocity range where the emission line of AAN was detected. We generated the integrated emission map only for the unblended transition of AAN towards G10. The integrated emission map indicated that the AAN molecule arises from the warm inner region of the hot core. We estimated the emitting region of AAN by fitting the 2D Gaussian over the integrated emission map of AAN using the `CASA` task `IMFIT` towards the G10. The deconvolved beam size of the emitting region was calculated by the following equation

$$\theta_S = \sqrt{\theta_{50}^2 - \theta_{beam}^2} \quad \text{Eq. 1}$$

where $\theta_{50}^2 = 2\sqrt{A/\pi}$ was the diameter of the circle whose area (A) was enclosing 50% line peak and θ_{beam} was the half-power width of the synthesized beam (Rivilla et al., 2017; Mondal et al., 2021). The estimated emitting region of AAN with transitions $J = 17(1,17)$ – $16(1,16)$, $J = 17(4,14)$ – $16(4,13)$, $J = 17(13,4)$ – $16(13,3)$, $J = 17(14,3)$ – $16(14,2)$, and $J = 18(0,18)$ – $17(0,17)$ were 1.12'', 1.13'', 1.11'', 1.12'', and

1.12'' respectively. So, the emitting region of AAN towards G10 varied between 1.11''–1.13''. After the fitting of the 2D Gaussian over the integrated emission map of AAN, we also estimated the integrated flux, peak flux, and position angle, which are presented in Table 2. We noticed that the emitting region of AAN is smaller than the synthesized beam size, which indicates the unblended transition lines of AAN are not well spatially resolved or, at best, marginally resolved.

3.3. Rotational diagram analysis of AAN

In this work, we have detected the multiple hyperfine transition lines of AAN towards G10. The rotational diagram method is one of the best ways to obtain the column density (N) in cm⁻² and rotational temperature (T_{rot}) in K of the detected emission lines of AAN. We assumed that the observed AAN spectra were optically thin and that they obeyed the Local Thermodynamic Equilibrium (LTE) conditions. The assumption of the LTE condition was reasonable towards the G10 because the density of the inner regions of the hot core was $\sim 7 \times 10^7$ cm⁻³ (Rolffs et al., 2011). The equation of column density can be written as in the case of optically thin lines (Goldsmith & Langer, 1999),

$$N_u^{thin} = \frac{3g_u k_B \int T_{mb} dV}{8\pi^3 \nu S \mu^2} \quad \text{Eq. 2}$$

where, k_B is the Boltzmann constant, $\int T_{mb} dV$ is the integrated intensity, μ is the electric dipole moment, g_u is the degeneracy of the upper state, ν is the rest frequency, and the strength of the transition lines were indicated by S . The total column density of detected species under LTE conditions can be written as,

$$\frac{N_u^{thin}}{g_u} = \frac{N_{total}}{Z(T_{rot})} \exp(-E_u/k_B T_{rot}) \quad \text{Eq. 3}$$

where $Z(T_{rot})$ is the partition function at extracted rotational temperature (T_{rot}). The rotational partition function at 75 K is 4403 and 150 K is 12460, respectively. The upper state energy of the observed molecular lines defined as E_u . In another way, the Eq. 3 can be rearranged as,

$$\ln \left(\frac{N_u^{thin}}{g_u} \right) = \ln(N) - \ln(Z) - \left(\frac{E_u}{k_B T_{rot}} \right) \quad \text{Eq. 4}$$

⁴Gorai et al. (2020) discussed the continuum emission towards G10 using ALMA

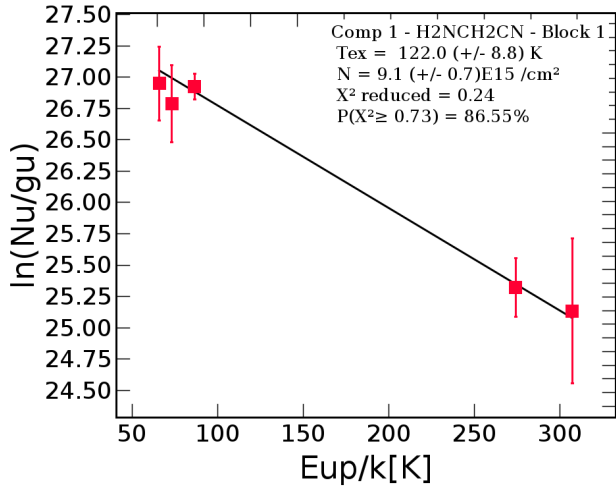


Figure 3: The rotational diagram of AAN towards G10. The red filled squares indicate the optically thin approximation data points and the red lines represent the error bars. The best-fit column density and rotational temperature are mentioned in the image.

Eq. 4 presented a linear relationship between the upper state energy (E_u) and $\ln(N_u/g_u)$ of the observed complex organic molecule AAN. The $\ln(N_u/g_u)$ were estimated from the Eq. 2. From Eq. 4, it is evident that spectral data points with respect to different transition lines of AAN should be fitted with a straight line whose slope is inversely proportional to T_{rot} , with its intercept yielding $\ln(N/Z)$, which in turn will help to estimate the molecular column density. During the rotational diagram analysis, we extracted the line parameters such as FWHM, upper energy (E_u), Einstein coefficients (A_{ij}), and integrated intensity ($\int T_{mb} dV$) using a Gaussian fitting over the observed transitions of AAN using the CASIS. The fitting parameters are presented in Table 1. We observed many transitions of AAN are blended as the present spectral resolution is not sufficient to resolve the hyperfine components. We used the most intense hyperfine transitions of AAN in our rotational diagram analysis. We have observed the maximum transitions of AAN blended with nearby molecular transitions. So, we used only unblended transitions of AAN during the rotational diagram analysis. The computed rotational diagram was shown in Figure 3. In the rotational diagram, the red error bars represent the absolute uncertainty of $\ln(N_u/g_u)$ originating from the error of the estimated integrated intensity, which was calculated after fitting the Gaussian model over the detected unblended emission lines of AAN. After the rotational diagram analysis, the estimated column density of AAN was $(9.10 \pm 0.7) \times 10^{15} \text{ cm}^{-2}$ with rotational temperature (T_{rot}) $122 \pm 8.8 \text{ K}$. The estimated fractional abundance of AAN was 7.01×10^{-8} where column density of H_2 towards G10 was $1.3 \times 10^{23} \text{ cm}^{-2}$ (Suzuki et al., 2016).

4. Discussion

4.1. AAN in the G10

The emission lines of AAN towards the hot molecular core G10 were the first time detected using ALMA with an estimated source size of $1.11''$ – $1.13''$ which is presented in this article. After the spectral analysis using the Gaussian model, it was found that the maximum transition lines of AAN were blended with nearby molecular lines as presented in Table 1. We observed that the $J = 17(1,17)$ – $16(1,16)$, $17(4,14)$ – $16(4,13)$, $17(13,4)$ – $16(13,3)$, $17(14,3)$ – $16(14,2)$, and $18(0,18)$ – $17(0,17)$ transition lines of AAN were not blended with nearby other molecular lines, and these transition lines were used during rotational diagram analysis to estimate the column density and gas temperature of AAN. The line contamination of AAN with other molecular lines towards G10 was less with respect to Sgr B2(N) because the estimated source size of G10 was $1.11''$ – $1.13''$ whereas the source size of Sgr B2(N) was $2''$. The estimated column density of AAN towards G10 was $(9.10 \pm 0.7) \times 10^{15} \text{ cm}^{-2}$ with rotational temperature (T_{rot}) $122 \pm 8.8 \text{ K}$, and corresponding line width 4 – 6 km s^{-1} with a centroid velocity 68.50 km s^{-1} . The fractional abundance of AAN with respect to H_2 was 7.01×10^{-8} where the column density of H_2 was $1.3 \times 10^{23} \text{ cm}^{-2}$ (Suzuki et al., 2016). The estimated rotational temperature indicated that the AAN molecule was mainly coming from the hot core of G10 because the temperature of the hot core was above 100 K (Rolffs et al., 2011). Earlier, the emission lines of AAN were detected from another hot molecular core Sgr B2(N) with fractional abundance 2.2×10^{-9} (Belloche et al., 2008). The fractional abundance of AAN in G10 was ~ 10 times higher than Sgr B2(N). In Sgr B2(N), the emission lines of AAN arise from the hot core region, which is also known as the ‘large molecule heimat’ (Belloche et al., 2008). Recently, Melosso et al. (2020) detected the emission lines of AAN from Sgr B2(N1S) using ALMA with ReMoCA spectral line survey and they estimated the column density of AAN was $1.1 \times 10^{17} \text{ cm}^{-2}$ with excitation temperature 200 K . The estimated column density of AAN derived from LTE modelling of ReMoCA spectral line survey toward Sgr B2(N1S) was $1.1 \times 10^{17} \text{ cm}^{-2}$, which was ~ 3.9 times higher than the column density reported in Belloche et al. (2008) for Sgr B2(N) from observations with the IRAM 30 m telescope. During the analysis of the column density of AAN, Belloche et al. (2008) and Melosso et al. (2020) both assumed the same emission size. There are several reasons for this difference. First of all, Belloche et al. (2008) did not account for the contribution of the vibrational partition function. They assumed the temperature of AAN was 100 K and this contribution amounts to a factor of 1.09 and after accounting for this, the column density derived from the IRAM 30 m data becomes $2.8 \times 10^{16} \text{ cm}^{-2}$.

4.2. Comparison with observation and simulated abundances of AAN

We compared our estimated abundance of AAN with the three-phase warm-up modelling results of Garrod (2013). Garrod (2013) assumed that there would be an isothermal

Table 3
Comparison between simulated and observed fractional abundances of AAN

Species	Simulated Values ^a						Observed Values ^b	
	Fast		Medium		Slow		G10	
	$f(\text{AAN})$	T (K)	$f(\text{AAN})$	T (K)	$f(\text{AAN})$	T (K)	$f(\text{AAN})$	T (K)
NH ₂ CH ₂ CN	4.3×10^{-9}	123	1.2×10^{-8}	122	4.7×10^{-9}	118	7.01×10^{-8}	122

Notes: a – Values taken from Table 8 of Garrod (2013);

b – this work.

collapse phase after a static warm-up phase. Under the free-fall collapse, the density increases from $n_H = 3 \times 10^3$ to 10^7 cm⁻³ in the first phase, and the temperature of the dust reduces to 8 K from 16 K. The temperature fluctuates from 8 K to 400 K in the second phase, but the density remains constant at $\sim 10^7$ cm⁻³ (Garrod, 2013). The temperature of G10 was ~ 150 K, which is a typical hot core temperature, and the number density (n_H) of this source is $\sim 10^7$ cm⁻³ (Rolffs et al., 2011; Gorai et al., 2020; Ohishi et al., 2019; Suzuki et al., 2016). Thus, the hot core model of Garrod (2013) is suitable for understanding the chemical evolution of AAN towards the G10. Garrod (2013) used the fast, medium, and slow warm-up models based on the time scale. In Table 3, we compared the observed fractional abundance of AAN with the three-phase warm-up model of Garrod (2013) and we observed that the simulation result was nearly similar to our observational results. We found that the medium warm-up model best matched the observation values of AAN towards the G10. During the comparison of the simulated and observed abundances of AAN, we found a tolerance of factor 7, which is a reasonably good agreement. Earlier, Ohishi et al. (2019) and Suzuki et al. (2016) claimed that the CH₂NH molecule obeys the medium warm-up model towards G10, and we observed that the AAN molecule also obeys the medium warm-up model towards G10. So, we conclude that both CH₂NH and AAN molecules obey the medium warm-up model towards G10. It is indicated that the CH₂NH molecule plays as a possible precursor of AAN towards G10. Earlier, another glycine precursor molecule, methylamine (CH₃NH₂) was also detected with column density $(1.0 \pm 0.7) \times 10^{15}$ cm⁻² from the G10 using the Nobeyama 45 m radio telescope. The detection of three possible glycine precursors like AAN (our work), CH₃NH₂ (Ohishi et al., 2019), and CH₂NH (Suzuki et al., 2016) towards G10 gives confidence in the possibility of the presence of interstellar glycine in this hot molecular core.

Garrod (2013) proposed that AAN is produced mainly by the addition of radical CH₂CN with NH₂, which is formed by hydrogen abstraction from CH₃CN molecules by NH₂ at around 60–80 K temperature, resulting in the fractional abundance of around 10^{-9} in the grain surface. Further, the evaporation of CH₃CN from the grains at a temperature of nearly 90 K produces CH₂CN with an efficiency of 50% with gas-phase protonation and electron recombination reactions. When this radical re-accretes to the grain surface and reacts with NH₂ then it produces a fractional abundance of AAN in the order of 10^{-8} . The estimated fractional abundance of AAN towards the G10 was 7.01×10^{-8} which indicated that

the proposed chemical modeling of Garrod (2013) satisfied the environment of G10.

4.3. Searching of interstellar glycine towards G10

After the successful detection of AAN, we also looked for the emission lines of glycine towards G10. After the deep searches of glycine conformer I and II using the LTE module in CASSIS, we did not detect this molecule within the limits of our LTE analysis. Using the same parameter of AAN ($\theta_S \sim 1.12''$ and $T_{ex} = 122$ K), the estimated upper limit column density of glycine conformer I was $\leq 1.25 \times 10^{15}$ cm⁻² and conformer II was $\leq 4.86 \times 10^{13}$ cm⁻². The energy of glycine conformer I is 705 cm⁻¹ (1012 K) lower than that of glycine conformer II (Lovas et al., 1995). The dipole moment of glycine conformer I is $\mu_a = 0.911$ D and $\mu_b = 0.607$ D, whereas conformer II is $\mu_a = 5.372$ D and $\mu_b = 0.93$ D (Lovas et al., 1995). In the interstellar medium, the a-type transitions of glycine are more prominent because the molecular line intensity is proportional to the square of the dipole moment (Lovas et al., 1995).

After the detection of CH₃NH₂ and CH₂NH towards G10, Ohishi et al. (2019) claimed that the hot molecular core G10 was one of the sources in an interstellar medium where glycine would be detectable. Our detection of AAN in G10 using ALMA gives more confidence that the hot molecular core G10 has the ability to form glycine. Earlier, Ohishi et al. (2019) estimated the upper limit column density of glycine conformer I with respect to CH₃NH₂ was $\leq 1.1 \times 10^{15}$ cm⁻² which satisfied our estimated upper limit column density of glycine with respect to AAN. We propose to conduct a survey of glycine conformer I and II and its precursors (CH₃NH₂, CH₂NH, AAN, and NH₂CH₂C(O)NH₂) molecules towards the hot molecular core G10 with a higher integration time and better spectral resolution to solve the puzzle of the glycine lines in the interstellar medium.

5. Conclusion

In this article, we presented the detection of the glycine nitrile molecule AAN towards G10 using ALMA band 4. The main results are as follows.

1. We successfully detected a total of twenty-one rotational emission lines of AAN towards the hot molecular core G10 using ALMA band 4 observation.
2. The derived column density of AAN using the rotational diagram method was $(9.10 \pm 0.7) \times 10^{15}$ cm⁻² with rotational

temperature 122 ± 8.8 K. The relative abundance of AAN with respect to H_2 was 7.01×10^{-8} where column density of H_2 in hot molecular core G10 was $1.3 \times 10^{23} \text{ cm}^{-2}$ (Suzuki et al., 2016).

3. In the discussion, we compared our fractional abundance of AAN with the three-phase warm-up model by Garrod (2013) and we found that the medium warm-up model satisfied our AAN abundance.

4. After the detection of AAN in G10, we also looked for the emission lines of glycine conformers I and II. Within the limits of our LTE analysis, we did not detect the emission lines of glycine conformer I and II towards G10. We calculated the upper limit column density of glycine conformer I as $\leq 1.25 \times 10^{15} \text{ cm}^{-2}$ and conformer II as $\leq 4.86 \times 10^{13} \text{ cm}^{-2}$.

5. After the unsuccessful detection of glycine conformers I and II using ALMA, we conclude that the emission line of glycine may be below the confusion limit in G10.

Acknowledgement

We thank both anonymous referee for helpful comments that improved the manuscript. The plots within this paper and other findings of this study are available from the corresponding author upon reasonable request. This paper makes use of the following ALMA data: ADS/JAO.ALMA #2017.1.00121.S. ALMA is a partnership of ESO (representing its member states), NSF (USA), and NINS (Japan), together with NRC (Canada), MOST and ASIAA (Taiwan), and KASI (Republic of Korea), in cooperation with the Republic of Chile. The Joint ALMA Observatory is operated by ESO, AUI/NRAO, and NAOJ.

Funding

This research did not receive any specific grant from funding agencies in the public, commercial, or not-for-profit sectors.

Declaration of Competing Interest

The authors declare that they have no known competing financial interests or personal relationships that could have appeared to influence the work reported in this paper

References

Alonso, E. R., Kolesniková, L., Białkowska-Jaworska, E., Kisiel, Z., León, I., Guillemin, J. C., Alonso, J. L., 2018. Glycinamide, a Glycine Precursor, Caught in the Gas Phase: A Laser-ablation Jet-cooled Rotational Study. *ApJ*, 861, 70.

Belloche, A., Müller, H. S. P., Garrod, R. T., Menten, K. M., 2016. Exploring molecular complexity with ALMA (EMoCA): Deuterated complex organic molecules in Sagittarius B2(N2). *A&A*, 587, A91.

Belloche, A., Menten, K. M., Comito, C., Müller, H. S. P., Schilke, P., Ott, J., Thorwirth, S., Hieret, C., 2008. Detection of amino acetonitrile in Sgr B2(N). *A&A*, 482, 179.

Bernstein, M. P., Ashbourn, S. F. M., Sandford, S. A., Allamandola, L. J., 2004. The Lifetimes of Nitriles (CN) and Acids (COOH) during Ultraviolet Photolysis and Their Survival in Space. *ApJ*, 601, 365.

Brown, R. D., Godfrey, P. D., Ottrey, A. I., Storey, J. M. V., 1977. Quadrupole hyperfine structure of the rotational spectrum of aminoacetonitrile. *Mol. Spectrosc.* 68, 359.

Danger, G., et al., 2011. Experimental investigation of aminoacetonitrile formation through the Strecker synthesis in astrophysical-like conditions: reactivity of methanimine (CH_2NH), ammonia (NH_3), and hydrogen cyanide (HCN). *A&A*, 535, A47.

Elsila, J., Dworkin, J. P., Bernstein, M. P., Martin, M. P., Sandford, S. A., 2007. Mechanisms of Amino Acid Formation in Interstellar Ice Analogs. *ApJ*, 660, 911.

Goldsmith, P. F., & Langer, W. D., 1999. Population Diagram Analysis of Molecular Line Emission. *ApJ*, 517, 209.

Gorai, P., Bhat, B., Sil, M., Mondal, S. K., Chakrabarti, S. K., Das, A., 2020. Identification of Prebiotic Molecules Containing Peptide-like Bonds in a Hot Molecular Core, G10.47+0.03. *ApJ*, 895, 86.

Garrod, R. T., 2013. A Three-phase Chemical Model of Hot Cores: The Formation of Glycine. *ApJ*, 765, 60.

Garrod, R. T., Belloche, A., Müller, H. S. P., Menten, K. M., 2017. Exploring molecular complexity with ALMA (EMoCA): Simulations of branched carbon-chain chemistry in Sgr B2(N). *A&A*, 601, A48.

Holtom, P. D., Bennett, C. J., Osamura, Y., Mason, N. J., & Kaiser, R. I., 2005. A Combined Experimental and Theoretical Study on the Formation of the Amino Acid Glycine (NH_2CH_2COOH) and Its Isomer ($CH_3NHCOOH$) in Extraterrestrial Ices. *ApJ*, 626, 940.

Jiménez-Serra, I., et al., 2020. Toward the RNA-World in the Interstellar Medium—Detection of Urea and Search of 2-Amino-oxazole and Simple Sugars. *Astrobiology*, 20, 9, 1048.

Kim, Y. S., & Kaiser, R. I., 2011. On the Formation of Amines (RNH_2) and the Cyanide Anion (CN^-) in Electron-irradiated Ammonia-hydrocarbon Interstellar Model Ices. *ApJ*, 729, 68.

Koch, D. M., Toubin, C., Peslherbe, G. H., Hynes, J. T., 2008. A Theoretical Study of the Formation of the Aminoacetonitrile Precursor of Glycine on Icy Grain Mantles in the Interstellar Medium. *J. Phys. Chem. C*, 112, 2972.

Kisiel, Z., et al., 2022. Millimetre-wave laboratory study of glycinamide and a search for it with ALMA towards Sagittarius B2(N). *A&A*, 657, A99.

Lovas, F. J., Kawashima, Y., Grabow, J. U., Suenram, R. D., Fraser, G. T., Hirota, E., 1995. Microwave Spectra, Hyperfine Structure, and Electric Dipole Moments for Conformers I and II of Glycine. *ApJ*, 455, L201.

McMullin, J. P., Waters, B., Schiebel, D., Young, W., & Golap, K., 2007. CASA Architecture and Applications. *Astronomical Society of the Pacific Conference Series*, Vol. 376, *Astronomical Data Analysis Software and Systems XVI*, ed. R. A. Shaw, F. Hill, & D. J. Bell, 127.

Manna, A., Pal, S., 2021. ALMA detection of ethyl cyanide and methyl formate in the hot molecular core IRAS 18566+0408. *arXiv:2105.01421*.

Mondal, S. K., et al., 2021. Is There Any Linkage between Interstellar Aldehyde and Alcohol?. *ApJ*, 2, 194.

Melosso, M., et al., 2020. Far-infrared laboratory spectroscopy of aminoacetonitrile and first interstellar detection of its vibrationally excited transitions. *A&A*, 641, A160.

Müller, H. S. P., Schilke, P., Stutzki, J., Winnewisser, G., 2005. The Cologne Database for Molecular Spectroscopy, CDMS: a useful tool for astronomers and spectroscopists. *Journal of Molecular Structure*, 742, 215.

Ohishi, M., Suzuki, T., Hirota, T., Saito, M., Kaifu, N., 2019. Detection of a new methylamine (CH_3NH_2) source: Candidate for future glycine surveys. *PASJ*, 71, 86.

Perley, R. A., & Butler, B. J., 2017. An Accurate Flux Density Scale from 50 MHz to 50 GHz. *ApJs*, 230, 1538.

Peltzer, E. T., Bada, J. L., Schlesinger, G. Miller, S. L., 1984. The chemical conditions on the parent body of the murchison meteorite: Some conclusions based on amino, hydroxy and dicarboxylic acids. *Advances in Space Research*, 4, 69.

Pickett, H. M., 1973. The microwave spectrum, structure, and dipole mo-

- ment of amino acetonitrile. *J. Mol. Spectrosc.* 46, 335.
- Rivilla, V. M., et al., 2017. Formation of ethylene glycol and other complex organic molecules in star-forming regions. *A&A*, 598, A59.
- Rolfs, R., Schilke, P., Zhang, Q., & Zapata, L., 2011. Structure of the hot molecular core G10.47+0.03. *A&A*, 536, A33.
- Rolfs, R., Schilke, P., Zhang, Q., Wyrowski, F., Menten, K., Zapata, L., 2009. Highly Excited HCN in the Massive Star Forming Region G10.47+0.0. *Submillimeter Astrophysics and Technology: a Symposium Honoring Thomas G. Phillips*, Astronomical Society of the Pacific Conference Series, 417, 215.
- Suzuki, T., Ohishi, M., Hirota, T., Saito, M., Majumdar, L., Wakelam, V., 2016. Survey Observations of a Possible Glycine Precursor, Methanimine (CH_2NH), *ApJ*, 825, 79.
- Sharma, M., 2019. Investigation of amino acetonitrile ($\text{NH}_2\text{CH}_2\text{CN}$)—a precursor of glycine, in the interstellar medium. *Canadian Journal of Physics*, 3, 98.
- Sanna, A., et al., 2014. Trigonometric parallaxes to star-forming regions within 4 kpc of the galactic center. *ApJ*, 781, 108.
- Theule, P., Borget, F., Mispelaer, F., Danger, G., Duvernay, F., Guillemin, J. C., Chiavassa, T., 2011. Hydrogenation of solid hydrogen cyanide HCN and methanimine CH_2NH at low temperature. *A&A*, 534, A64.
- Vastel, C., Bottinelli, S., Caux, E., Glorian, J. -M., Boiziot, M., 2015. CAS-SIS: a tool to visualize and analyse instrumental and synthetic spectra. *Proceedings of the Annual meeting of the French Society of Astronomy and Astrophysics*, 313-316.
- Wirström, E. S., Bergman, P., Hjalmarson, Å, Nummelin, A., 2007. A search for pre-biotic molecules in hot cores. *A&A*, 143, 177.
- Woon, D. E., 2002. Pathways to Glycine and Other Amino Acids in Ultraviolet-irradiated Astrophysical Ices Determined via Quantum Chemical Modeling. *ApJ*, 571, L177.